Wetlands (2020) 40:939–956
https://doi.org/10.1007/s13157-020-01284-7

APPLIED WETLAND SCIENCE

Modeling the Spatio-Temporal Evolution of Chlorophyll-*a* in Three Tropical Rivers Comoé, Bandama, and Bia Rivers (Côte d'Ivoire) by Artificial Neural Network

Maley-Pacôme Soro[1,2] · Koffi Marcellin Yao[2] · N'Guessan Louis Berenger Kouassi[3] · Ahmed Abauriet Ouattara[1,2] · Thomas Diaco[1]

Received: 2 August 2019 / Accepted: 21 February 2020 / Published online: 6 March 2020

Abstract

Rivers and their watersheds play a key role in the global biogeochemical cycle of nitrogen and phosphorus in the biosphere. They are also important economic resources for humans. However, little information is available on eutrophication of West African coastal rivers due to costly analytical instruments and socio-economic difficulties. In this study, the spatial distributions of chlorophyll-*a* biomass in the Comoé, Bandama, and Bia Rivers (Côte d'Ivoire) were mapped during the dry, rainy and flood seasons, and chlorophyll-*a* dynamics were simulated using Artificial Neural Network (ANN) models. The results showed a state of advanced eutrophication during the three sampling seasons. The best generalizable models obtained from the data collected during 2 years and covering three hydrological seasons of the rivers forecasted between 76% and 85% of present chlorophyll-*a* concentrations (static approach), and between 73% and 84% of future chlorophyll-*a* concentrations (both dynamic t and t + 1 approaches). These models achieved satisfactory accuracy with low relative mean errors (MRE) ranging from 3.22% to 7.71%. The results of this study suggest that ANN model could be an original and less expensive tool for monitoring river water eutrophication in developing countries.

Keywords Modeling eutrophication · Artificial neural network · River · Côte d'Ivoire

Introduction

Eutrophication of surface waters such as rivers is one of the most common environmental problems in the world in terms of water quality. The main consequences of the excess of nutrients in lakes, coastal waters, large rivers or small streams are hypoxia/anoxia, increase of primary production (abundant algae growth) followed by increase of turbidity, disturbance of the aquatic ecosystems equilibrium, among others which are direct consequences of eutrophication (Gibson et al. 2000; Yasin et al. 2010; Chen et al. 2016). The European Environmental Agency defines eutrophication as an increase in the rate of organic matter supply to an ecosystem, which most commonly is related to nutrient enrichment enhancing the primary production in the system (EEA 2001). Often, rivers are important conduit of nutrients but algal production may be very low due to light limitation (from turbidity or forest cover), or high river velocity upstream. In contrast, eutrophication is more pronounced in rivers' delta, estuaries, and in lakes. The trophic state of lakes and tropical rivers is usually classified into six grades based on chlorophyll-*a* concentrations: 0–1.6 μg/L representing oligotrophic, 1.6–10 μg/L mesotrophic, 10–26 μg/L light-eutrophic, 26–64 μg/L mid-eutrophic, 64–160 μg/L high-eutrophic, and > 160 μg/L hypereutrophic (Jin and Tu 1990; Huo et al. 2013). The increasing high anthropogenic inputs of nutrients in river watersheds are well known as the main culprit of eutrophication (Aguiar et al. 2011; N'goran et al. 2019). Therefore, it is

Electronic supplementary material The online version of this article (https://doi.org/10.1007/s13157-020-01284-7) contains supplementary material, which is available to authorized users.

✉ Koffi Marcellin Yao
markcelklindr@gmail.com; ykmarco21@yahoo.fr

[1] Laboratoire de Chimie Physique, Université Félix Houphouët Boigny, 22 BP 582, Abidjan, Côte d'Ivoire

[2] Centre de Recherches Océanologiques (CRO), 29, rue des pêcheurs, BP V18, Abidjan, Côte d'Ivoire

[3] UFR des Sciences Biologiques, Université Péléforo Gon Coulibaly, BP 1328, Korhogo, Côte d'Ivoire

necessary to monitor the evolution of eutrophication for the preservation of the freshwater quality.

Many indices such as the trophic indexes (TRIX, TLI, and TSI) have been used for both the monitoring of the surface water quality and classification of river and lake trophic levels using the chlorophyll-*a*, nutrients concentrations along with a few physicochemical parameters (Pesce and Wunderlin 2000; Moscuzza et al. 2007; Pettine et al. 2007; Cunha et al. 2013; Huo et al. 2013; Ota et al. 2015; Singh and Singh 2015; Wu et al. 2018). Through linear regression, these indexes provide an insight on how nutrient (i.e., dissolved inorganic nitrogen, reactive phosphorus, total phosphorus), light availability and other factors (e.g., dissolved oxygen, potassium permanganate) stimulate algal biomass development (usually measured as chlorophyll-*a*, Chl-*a*) and contribute to the increase of the aquatic systems enrichment condition (Primpas and Karydis 2010; Cunha et al. 2013; Li et al. 2017).

However, the prediction of eutrophication from these indices remains difficult given the interdependence and complexity of climatic, geographical and ecological factors affecting this phenomenon. Artificial Neural Network (ANN) is an increasingly popular alternative in environmental modeling because of its high potential for predicting complex relationships with precise accuracy (Sudheer et al. 2002; Sudheer and Jain 2004; Lohani et al. 2011; Wu et al. 2013; Wu et al. 2014; Huang and Gao 2017; Chen et al. 2018). ANNs are mathematical tools whose functioning is inspired by that of the human brain. Like their biological counterpart, neurons in layers receive, treat (by weighted summation), and transfer information generally via a nonlinear function (Assidjo et al. 2008). It has been demonstrated that ANNs are better than many linear and mechanistic regression models because of their ability to simulate non-linear phenomena including algal bloom dynamics and dissolved oxygen (DO) from water quality monitoring data. For example, Muller and Muller (2015) forecasted estuarine hypoxia in the main-stem of the Chesapeake Bay using a wavelet based ANN model. Chang et al. (2015) used ANNs to successfully forecast the low flow velocity regime in a constructed wetland in the Florida Everglades. Huo et al. (2013) predicted eutrophication with indicators such as DO, total nitrogen (TN), chlorophyll-*a* (Chl-*a*) and secchi disk depth (SD) with reasonable accuracy in Lake Fuxian, the deepest lake of southwest China, while Huang and Gao (2017) simulated chlorophyll-*a* in Lake Poyang in China using ANN models. However, studies in tropical regions are concentrated primarily in Asia, and limited data is available for West African rivers (Awad 2014; Wang et al. 2015; Tian et al. 2017; Hao et al. 2019). As an example, in Côte d'Ivoire, studies on eutrophication modeling have been conducted only in lagoons (Yao et al. 2017). Given that river waters are vital for people in rural areas, prediction of eutrophication in these waters is necessary. The aim of this study was to model the spatio-temporal evolution of chlorophyll-*a*, the main indicator of eutrophication using Artificial Neural Network in three typical rivers of Côte d'Ivoire (The Comoé, Bandama and Bia Rivers) which are used for drinking, fishing, bathing, and irrigation by the local populations without any treatment. One of the main detrimental effects of eutrophication is the increased occurrence of harmful algae, especially Cyanobacteria which can present chronic health risks to humans (Le Moal et al. 2019). For example, liver cancer was observed in a population from central Serbia following the consumption of water contaminated by Cyanobacteria (Svirčev et al. 2009). Secondly, eutrophication of these three rivers could result in socio-economic impacts such as cost of water treatment and financial problems for fishing communities. From field data, simulations for different rivers were made; then, the adequacy between predicted and target data was discussed.

Materials and Methods

Study Area and Samplings

The present study was conducted on three main rivers: the Comoé, Bandama and Bia Rivers which irrigate southeastern Côte d'Ivoire (Fig. 1). The Comoé River originates from the Banfora region in Burkina Faso and traverses 1160 km in Côte d'Ivoire before discharging into Ebrié Lagoon and the Gulf of Guinea. It has an annual average flow of about 106 m^3/s and a drainage basin of 82,408 km^2. The Bandama River takes its source in the northern Côte d'Ivoire, between Korhogo and Boundiali at an altitude of 480 m and flows into Grand-Lahou Lagoon and the Gulf of Guinea in the South. With a length of 1050 km, its catchment area covers 97,500 km^2 with an annual average discharge about 263 m^3/s.

The hydrological regime of the Comoé and Bandama Rivers is essentially a tropical transitional regime with a single flood from August to October, and a long period of low water from January to May (Fig. 2).

The Bia River is a small river located in the southeast corner of Côte d'Ivoire. It originates from Ghana in north of Chemraso, flows southward and discharges into Aby Lagoon. The length of the Bia River is about 120 km in Côte d'Ivoire, and the annual average discharge is 104 m^3/s. The Bia River is linked to an equatorial transition regime marked by two annual floods. The first (usually the strongest) and second floods, occur during the June–July period and the October–November period, respectively (Durand et al. 1994; Girard et al. 1970).

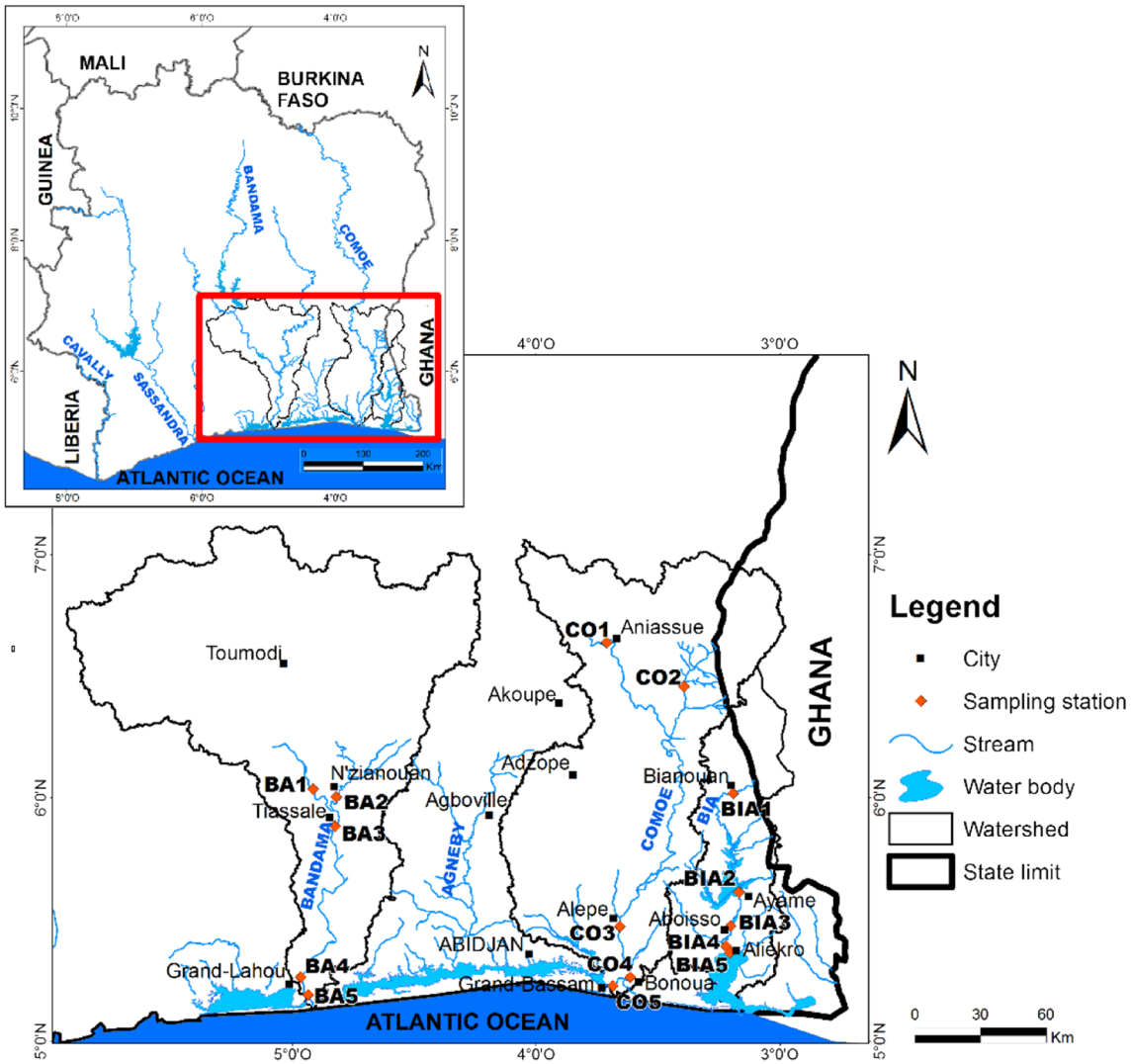

Fig. 1 Sampling stations along the Comoé, Bandama and Bia Rivers

Four climatic seasons occur in the study area: a long dry season (December–March), a long rainy season (April–July), a short dry season (August-middle September) and a short rainy season (Middle September–November).

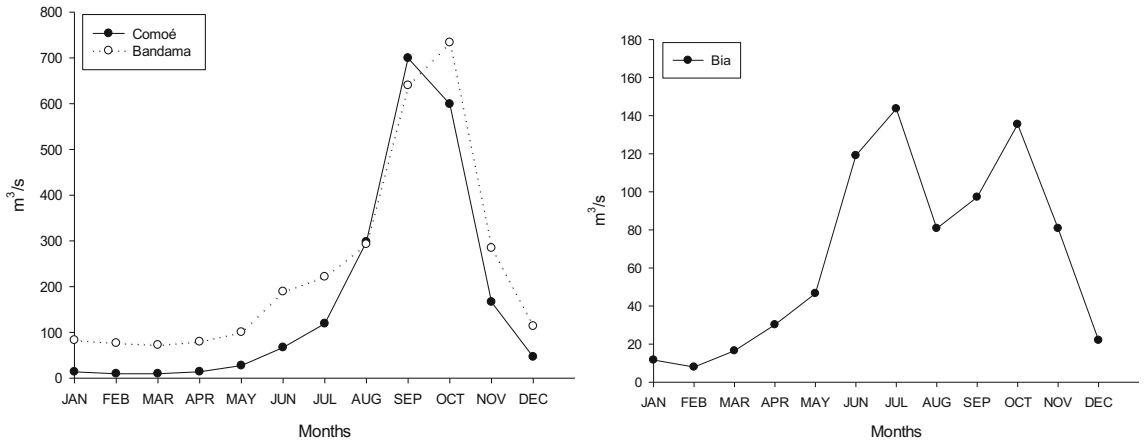

Fig. 2 Annual discharges of the Comoé, Bandama and Bia Rivers

Six sampling campaigns were conducted in the Comoé, Bandama and Bia Rivers from March 2016 to November 2017 during the dry, rainy and flood seasons. Five stations were sampled in the Comoé River from station CO1 to station CO5, five in the Bandama River from station BA1 to station BA5, and five in the Bia River from station BIA1 to station BIA5 (Table 1).

Procedure, Reagents and Quality Assurance

A Multiparameter Meter with GPS - HANNA HI 9828 was used to measure in situ parameters including temperature, pH, salinity, conductivity and dissolved oxygen. Water samples were collected with a 2.5 L Niskin bottle at 0.3 m below the surface of the streams. Water samples were filtered through a 0.45 μm Whatman GF/C filter and then stored in polyethylene flasks of 1 L volume (previously washed with 10% HCl and rinsed three times with ultrapure water). Subsequently, these flasks were acidified with sulfuric acid or hydrochloric acid, then stored at 4 °C and protected from light in a cooler. Analyses were performed within 72 h in the laboratory. Nutrients and chlorophyll-*a* analyses were performed according to Rodier et al. (2009) reference method. A portable spectrophotometer (HACH model DR/2400) was used for analysis (Koroleff 1970 for ammonium ion measurements; Grasshoff et al. 1999 for nitrates and Murphy and Riley 1962 for phosphates). Chlorophyll-*a* was extracted with 90% acetone in the dark and analyzed by Lorenzen's method (Lorenzen 1967). Blanks were analyzed in each batch of water samples throughout the entire analytical procedure. The accuracy and precision of the results were checked by triplicate measurements. The detection limits were 0.004 mg/L for PO_4^{3-}, 0.002 mg/L for NH_4^+, 0.005 mg/L for NO_3^- and 0.1 μg/L for Chl-*a*. The errors in analyses in terms of standard deviations of triplicate samples were found to be 0.001, 0.005, 0.02 mg/L and 0.38 μg/L for PO_4^{3-}, NH_4^+, NO_3^- and Chl-*a*, respectively.

Data Set

The time-series data collected during the 2 years allowed for a characterization of water physico- chemical parameters and the chlorophyll-*a* (Chl-*a*) values in the Comoé, Bandama and Bia Rivers (Table 2). The data set consisted of 150 measurements per parameter. These parameters (predictors) can interact with the chlorophyll-*a* dynamics in rivers. We investigated the presence of associations between both predictor and response variables by calculating Pearson and Spearman correlation coefficients between all possible combinations of variables. The correlation coefficients estimated between predictors and the response variable (Chl-*a*) demonstrated that many of the predictor-response associations were nonlinear, as evidenced by the values of the Pearson correlation scores being lower than the Spearman correlation scores (Tables S1 to S3). This result suggested that such associations between predictor variables and the response should not be modeled with linear models. Therefore, ANNs are an ideal alternative to model these relationships as they are better suited to

Table 1 Geographical locations of sampling stations and sampling period

					2016			2017		
					Hydrological seasons of rivers					
River		Area	Latitude N	Longitude W	Dry 1st sampling	Rainy 2nd sampling	Flood 3rd sampling	Dry 1st sampling	Rainy 2nd sampling	Flood 3rd sampling
Bandama	BA1	Bafécao	6.035757	−4.916859	2016/03/18*	2016/06/09	2016/10/06	2017/03/15	2017/06/15	2017/11/17
	BA2	N'zi	6.00297	−4.822094						
	BA3	Tiassalé	5.883404	−4.825975						
	BA4	Lahou	5.263395	−4.967991						
	BA5	Braffedon	5.144469	−4.971661						
Comoé	CO1	Aniassué	6.638662	−3.711774	2016/03/17	2016/06/08	2016/10/05	2017/03/14	2017/06/14	2017/11/16
	CO2	Manzan	6.458642	−3.394239						
	CO3	Alepe	5.30091	−3.393094						
	CO4	Bonoua	5.262114	−3.613791	2016/03/16	2016/06/07	2016/10/04	2017/03/13	2017/06/13	2017/11/15
	CO5	Bassam	5.226616	−3.68545						
Bia	BIA1	Bianoua	6.019232	−3.191507						
	BIA2	Ayamé	5.612799	−3.167517						
	BIA3	Aboisso	5.474137	−3.202904						
	BIA4	Krindjabo	5.389706	−3.221596						
	BIA5	Thomandié	5.362501	−3.205251						

*yy/mm/dd

Table 2 Range, mean, standard deviation and relative standard deviation for water quality data, meteorological data and chlorophyll-*a* in the three sampled rivers between 2016 and 2017

		Predictors										Response
		Water quality data								Meteorological data		
River	Statistics	Temp. (°C)	pH	EC (μS/cm)	DO (mg/L)	Sal. (psu)	PO_4^{3-} (mg/L P)	NO_3^- (mg/L NO_3^--N)	NH_4^+ (mg/L NH_3-N)	Discharge (m^3/s)	Pluviometry (mm)	Chl-*a* (μg/L)
Comoé	Min-Max	26.50–30.97	6.49–7.92	15.00–126.00	2.58–8.35	0.01–0.06	0.01–0.10	0.02–1.90	0.02–0.62	9.50–599.17	114.62–304.59	0.68–164.16
	Mean	28.94	7.22	55.59	4.78	0.03	0.06	0.60	0.08	225.19	187.49	45.44
	SD	1.19	0.41	29.69	1.57	0.01	0.03	0.48	0.11	270.02	85.06	48.63
	RSD (%)	4.11	5.64	53.40	32.76	49.85	55.63	79.19	137.41	119.91	45.37	107.04
Bandama	Min-Max	28.25–33.43	6.67–8.04	30.00–1265.42	2.66–6.71	0.00–9.03	0.01–0.12	0.21–3.60	0.01–0.52	72.29–733.54	98.18–449.01	0.95–143.91
	Mean	30.22	7.38	148.35	5.04	0.50	0.05	0.98	0.08	331.67	234.49	43.32
	SD	1.56	0.39	244.28	1.04	1.84	0.04	0.70	0.09	293.07	156.16	38.49
	RSD (%)	5.17	5.22	164.66	20.67	367.08	75.69	71.14	115.00	88.36	66.59	88.87
Bia	Min-Max	24.85–30.86	6.48–8.39	15.00–82.00	3.21–7.63	0.01–0.04	0.01–0.11	0.08–1.40	0.01–0.16	16.56–135.46	118.79–236.59	1.80–92.61
	Mean	27.99	7.52	44.63	5.46	0.02	0.06	0.58	0.06	90.36	171.59	25.77
	SD	1.65	0.43	18.49	0.87	0.01	0.04	0.30	0.04	53.51	49.69	24.01
	RSD (%)	5.91	5.73	41.43	15.94	46.09	61.90	51.33	64.70	59.22	28.96	93.19

account for the non-linear associations between the response and the interactions among predictors (Li et al. 2013).

Neural Network

Artificial Neural Network (ANN) Model Development

Finding neural network models includes computing appropriate weights and biases that minimize the discrepancy between observed and simulated data. Development of artificial neural networks were performed based on the Matlab neural network toolbox R2018a Software. During all simulations, the Levenberg-Marquardt algorithm (Levenberg 1944; Marquardt 1963) was used to accelerate the training step. Artificial neural network models were built to predict chlorophyll-*a* concentration. The simulations were carried out initially with as predictors, all the ten parameters measured (Temperature, pH, EC, DO, salinity, PO_4^{3-}, NO_3^-, NH_4^+, river discharge, and pluviometry). Two approaches were considered in this study (Fig. 3). First of all, the static modeling of the chlorophyll-*a* was performed using ten predictors constituting the input parameters X_i and measured chlorophyll-*a* values in the river as the output parameter Y_i. Then, the dynamic models of chlorophyll-*a* were performed adding the time, namely the month of the season during which the sampling was conducted, to the ten previous predictors. The response $Y_i(t)$ represents the forecasting chlorophyll-*a* concentration in the river for the current season while the response $Y_i(t+1)$ represents the chlorophyll-*a* concentration for the next season in the river. It should be noted that the static modeling approach forecasts the present values of chlorophyll-*a* without including the time (month) as an input parameter, while the dynamics modeling approaches forecast the future values of chlorophyll-*a* (Fig. 3).

To form the network, data were randomly and evenly divided into three subsets by the calculation algorithm: training (50% of data), testing (25% of data) and validation (25% of data). The training subset is used for computing and updating the network weights and biases (Assidjo et al. 2008). The error in the testing set is monitored during the training process. The testing error will normally decrease during the initial phase of training, as does the training set error. However, when the network begins to overfit the data, the error in the testing set will typically begin to increase. When the testing error increases for a specified number of iterations, the training is stopped and the weights and biases of the minimum testing error are returned. The validation data set are only used to test the final solution in order to assess the performance of the network (Assidjo et al. 2008).

All inputs were normalized using the following formula:

$$x_{ni} = \frac{2(x_i - x_{min})}{(x_{max} - x_{min})} - 1 \quad (1)$$

Where x_{ni} is the normalized data ranging between −1 and 1, x_i is the initial data, and x_{min} and x_{max} are minimum and maximum values of the data set.

The network architecture has been optimized by varying the hidden layer neurons number from 1 to 15 taking into account the highest correlation coefficients of training (R_{app}) and validation (R_{val}) phases, but also the lowest values of the mean squared errors (MSE). For each hidden neuron, simulations were carried out 1500 × 5 times by randomly generating weights and the best result of the corresponding network architecture has been registered. The transfer function of hidden layer nodes was the tanh function and the linear function for the output layer (Lee et al. 2016). Every hidden neuron produces an output y'_j according to Eq. 2:

$$y'_j = \tanh\left(\sum w_{ij} x_i + b_j\right) \quad (2)$$

Where w_{ij} represents the weights, x_i the inputs, b_j the bias associated with the output y'_j and tanh is the transfer function between the input layer and the hidden neuron.

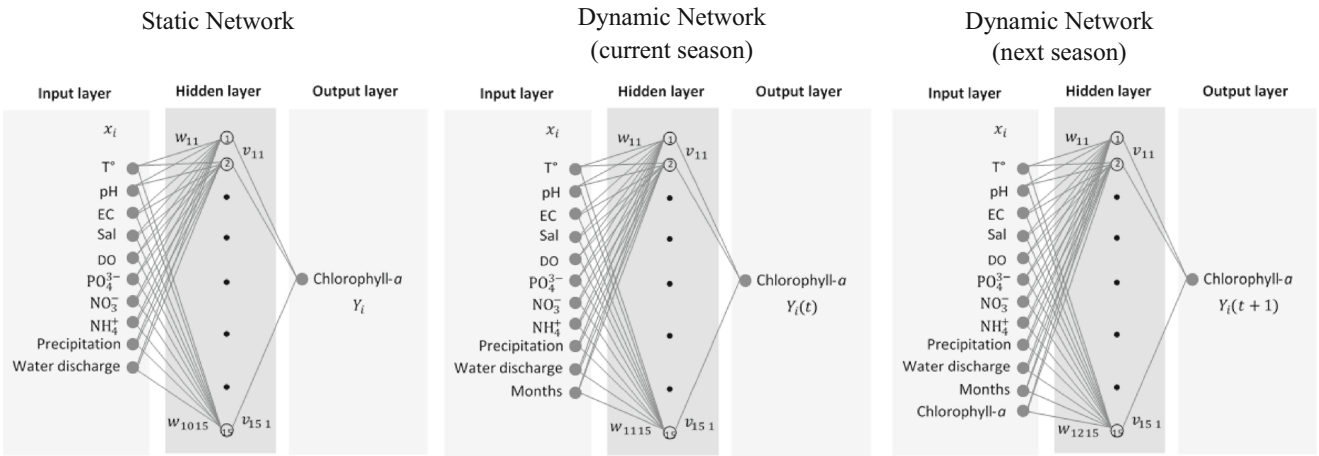

Fig. 3 Structures of the Artificial Neural Network (ANN)

Each output neuron produces an output value Y_i which represents the predicted value of chlorophyll-*a* according to Eq. 3:

$$Y_i = \sum\left(v_{ij} y'_j\right) + b_i \quad (3)$$

Where v_{ij} represents the weights, y'_j the hidden neurons and b_i the bias associated with the output Y_i (Assidjo et al. 2008).

ANNs models obtained appeared quite complex with sometimes up to 13 neurons in the hidden layers. It was necessary to carry out tests to ensure that there was no overfitting. Thus, the relevance of the input variables of the ANN models was estimated according to the Olden method (Olden et al. 2004) for chlorophyll-*a* prediction in each river. Connection weight approach of Olden et al. (2004) calculates the product of the raw input-hidden and hidden-output connection weights between each input neuron and output neuron and sums the products across all hidden neurons (Plate 1 in supplementary files). This approach assigned importance values to the predictors that were proportional to their influence on the output of the model. These values were above zero if the predictor had a positive association with the response variable and below zero if the predictor had a negative association with the response variable (Coutinho et al. 2019). Networks with values of importance assigned to predictors below −0.5 or above +0.5 were considered valid, in order to exclude overly complex models. This filtering criteria gives the best results and reduces to a maximum to 6, the number of neurons on the hidden layer in the final models. When two predictor values presented close importance or a linear correlation (Pearson), a preferential choice was made for the one with the highest importance. This would reduce the networks size at most six predictors on the input layer, and that would provide a nice trade-off between predictive powers while avoiding overfitting. Thus, the simulations were redone 1500 × 5 times with the predictors selected at the input by randomly generating new weights, and the best result of the corresponding network architecture was registered. The raw data was provided in Tables S4 to S6 (supplementary files).

The principal component analysis (PCA) was also, applied to data from the Comoé, Bandama and Bia Rivers (1650 measurements per river) to examine potential factors driving the physical and chemical parameters. The PCA was performed using Statistica® version 7 software. All graphs were performed using Sigmaplot® version 12.0 and 14.0.

Model Performance

Evaluation of the model performance consists in judging its ability to predict chlorophyll-*a* dynamics in the Comoé, Bandama and Bia Rivers. The ANN program calculated the correlation coefficients for the training (R_{app}) and validation (R_{val}) sets and the mean square errors for the training (MSE_{app}) and validation (MSE_{val}) sets. The best networks were selected among those that achieve the highest performance (i.e., high R_{app} and R_{val} with low MSE_{val} values) without overfitting (i.e., adequate fits for both training and validation sets). In all, 225 ANNs were built for each river after the simulations. Networks were considered valid if they were characterized by $R_{app} > 0.5$; $R_{val} > 0.5$ and $MSE < 1$ (Coutinho et al. 2019).

Another approach is determination of Schwarz's Bayesian information criterion (BIC) (Schwarz 1978; Assidjo et al. 2008) obtained as follows:

$$BIC = \log(MSE) + p\,\frac{\log(n)}{n} \quad (4)$$

Where MSE is mean squared errors, n the number of training patterns and p the total number of network weights. So the smallest BIC would give the best generalizable model.

The mean relative error (MRE) is also introduced to evaluate the performance of ANN models and to estimate whether the obtained model is generalizable (Xu et al. 2015).

$$MRE = \frac{1}{n}\sum_{i=1}^{n}\left|\frac{Y_{pr} - Y_{obs}}{Y_{obs}}\right| \times 100 \quad (5)$$

Where n is the number of the samples in test set.

From eq. (5), it is obvious that the smaller the MRE is, the better generalization is achieved (Xu et al. 2015).

Results and Discussion

Chlorophyll-*a* Dynamics

The spatio-temporal distributions of the chlorophyll-*a* in the Comoé, Bandama, and Bia Rivers during the dry, rainy and flood seasons are shown in Fig. 4. Thematic maps were computed using the ArcGIS/ArcMap environment based on Inverse Distance Weighting (IDW) interpolation. The seasonal variation of phytoplankton biomass distributions, expressed as chlorophyll-*a* showed no clear trend over the study period (March 2016 to November 2017) at the three sites as a result of urban and agricultural inputs. Very high chlorophyll-*a* concentration (164 μg/L) was observed during the flood season at the mouth of the Comoé River (CO5), while a very low value (6.20 μg/L) was obtained in the same river at Bonoua station (CO4) during the flood season. Strong proliferation of phytoplankton had been noted in the estuarine part of the three rivers during the three seasons because rivers are often important conduit of nutrients to downstream habitats (Yasin et al. 2010). Yet, this proliferation was not pronounced upstream especially during the dry and flood seasons, except at the Manzan station (CO2) where rainwater runoffs loaded in nitrates led to an increase in photosynthetic activity (de Sousa

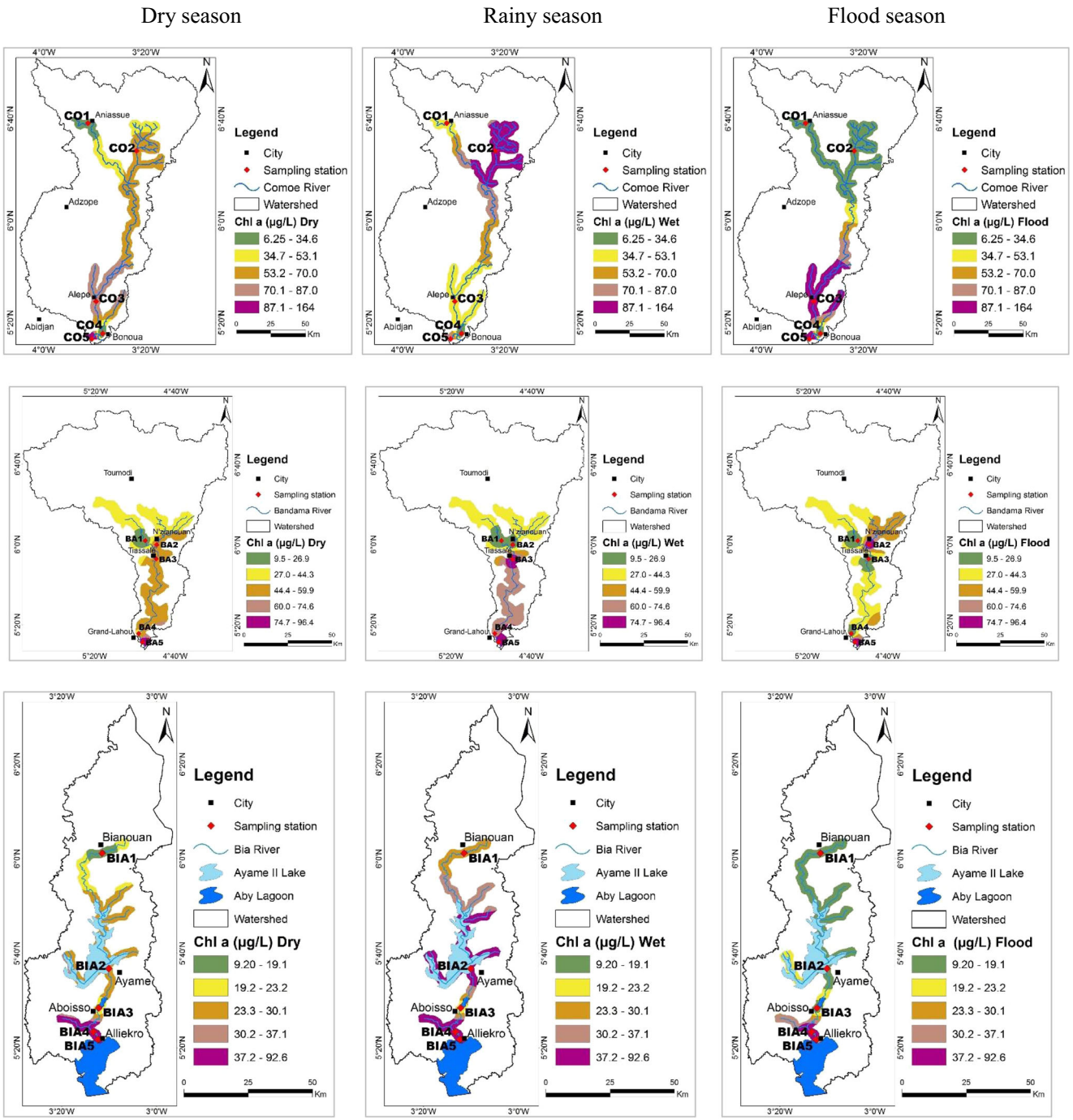

Fig. 4 Spatio-temporal chlorophyll-*a* dynamics in the Comoé, Bandama and Bia Rivers from March 2016 to November 2017. Data plotted are average concentrations obtained from March 2016 and March 2017 during the dry season, June 2016 and June 2017 during rainy season, and October 2016 and November 2017 during flood season

Barroso et al. 2016). Pearson correlation analyses were performed to test for associations between chlorophyll-*a* abundance and measured environmental parameters, especially nitrate and phosphate. (Tables S1 to S3). Chlorophyll-*a* correlated positively with phosphates in the Bandama and Bia Rivers and with nitrates in the Comoé River. The river discharge and dissolved oxygen (DO) correlated negatively with chlorophyll-*a* in the Bandama and Bia Rivers, respectively. The lower yet significant Pearson correlation scores observed (range: - 0.236 to +0.433) suggest that the variation of these nutrients and physicochemical parameters could linearly account for the chlorophyll-*a* values. The chlorophyll-*a* values increased with phosphate inputs in the Bandama and Bia Rivers, and nitrate increased with chlorophyll-*a* in the Comoé River mainly in the rainy season. This result could indicate a limitation of nitrogen in the Comoé River and

Table 3 The classification scheme for Chl-*a* biomass in the Comoé, Bandama and Bia Rivers according to the classification of the European Environmental Agency (EEA 2001). Data are average concentrations obtained from March 2016 and March 2017 during the dry season, June 2016 and June 2017 during rainy season, and October 2016 and November 2017 during flood season

Classification of the European Environmental Agency (EEA 2001)							
Chl-*a* (μg/L)	0–1,6		1,6–10	10–26	26–64	64–160	>160
Trophic state	Oligotrophic		Mesotrophic	Light-eutrophic	Mid-eutrophic	High-eutrophic	Hypereutrophic
Assessment of the trophic state of rivers according to the classification of EEA (2001)							
River		Dry		Rainy		Flood	
		Chl-*a* (μg/L)	Trophic state	Chl-*a* (μg/L)	Trophic state	Chl-*a* (μg/L)	Trophic state
Comoé	CO1	29.84	Mid-eutrophic	47.25	Mid-eutrophic	12.42	Light-eutrophic
	CO2	55.49	Mid-eutrophic	103.68	High-eutrophic	7.29	Mesotrophic
	CO3	84.02	High-eutrophic	48.87	Mid-eutrophic	119.16	High-eutrophic
	CO4	12.69	Light-eutrophic	19.17	Light-eutrophic	6.21	Mesotrophic
	CO5	123.93	High-eutrophic	83.70	High-eutrophic	164.16	Hypereutrophic
	BA1	13.01	Light-eutrophic	15.93	Light-eutrophic	10.08	Light-eutrophic
	BA2	55.62	Mid-eutrophic	20.52	Light-eutrophic	90.72	High-eutrophic
Bandama	BA3	51.30	Mid-eutrophic	89.37	High-eutrophic	13.23	Light-eutrophic
	BA4	39.96	Mid-eutrophic	70.47	High-eutrophic	9.45	Mesotrophic
	BA5	91.67	High-eutrophic	86.94	High-eutrophic	96.39	High-eutrophic
	BIA1	18.50	Light-eutrophic	27.81	Mid-eutrophic	9.18	Mesotrophic
	BIA2	26.87	Mid-eutrophic	40.77	Mid-eutrophic	12.96	Light-eutrophic
Bia	BIA3	18.23	Light-eutrophic	19.17	Light-eutrophic	17.28	Light-eutrophic
	BIA4	39.33	Mid-eutrophic	34.56	Mid-eutrophic	44.10	Mid-eutrophic
	BIA5	64.40	High-eutrophic	92.61	High-eutrophic	36.18	Mid-eutrophic

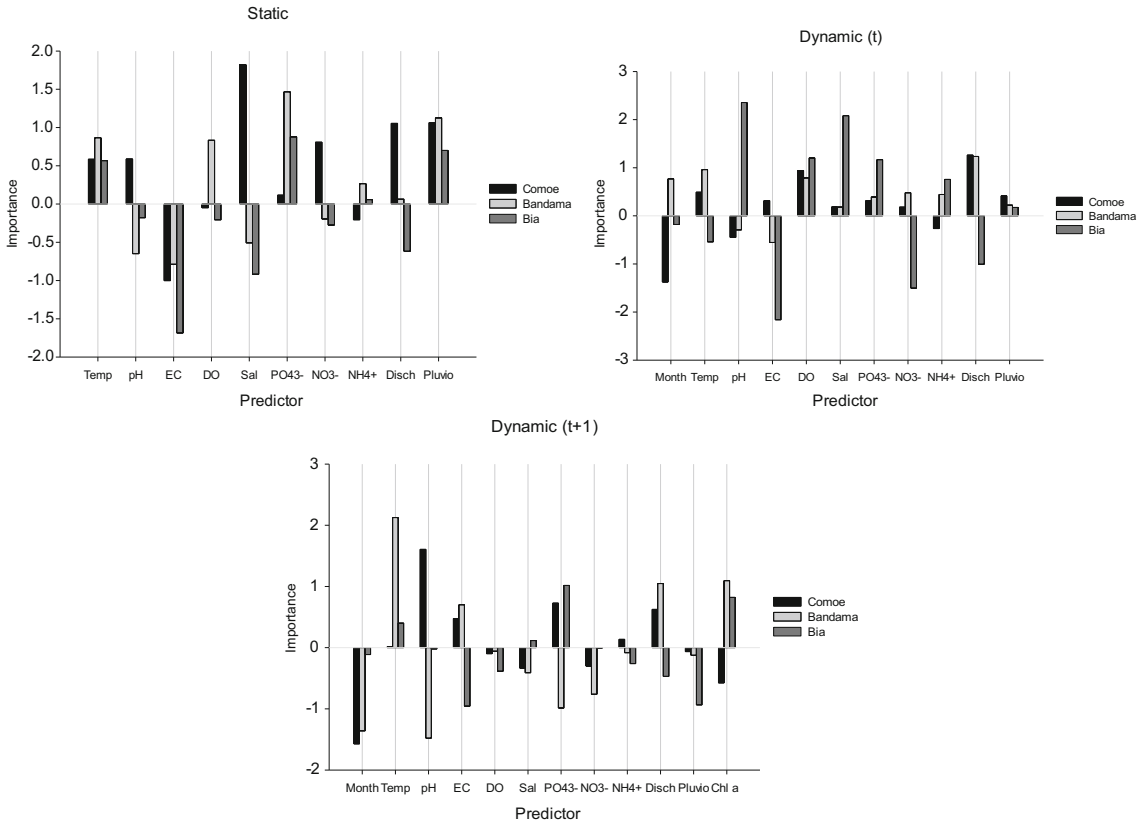

Fig. 5 Bar plot depicting the relative importance of predictors for the response estimated from ANN weights through the Olden method

Table 4 Performance and variable importance for the best performing networks for chlorophyll-*a* prediction. The rank of predictor variable importance is included above the first and the last variables

	Static approach			Dynamic (t) approach			Dynamic (t + 1) approach		
	Predictor importance (rank)	Performance		Predictor importance (rank)	Performance		Predictor importance (rank)	Performance	
		R_{val}	MSE_{val}		R_{val}	MSE_{val}		R_{val}	MSE_{val}
Comoé	[1]Sal, Disch, EC, NO_3^-,[5]pH	0.75	0.09	[1]Month, Disch, DO, [4]Temp	0.82	0.11	[1]Month, pH, PO_4^{3-}, Disch, [5]Chl-*a*	0.63	0.13
Bandama	[1]PO_4^{3-}, Pluvio, Temp, DO, EC, [6]pH	0.67	0.15	[1]Disch, Temp, DO, Month, [5]EC	0.66	0.22	[1]Temp, pH, Month, Chl-*a*, Disch, [6]PO_4^{3-}	0.68	0.21
Bia	[1]EC, PO_4^{3-}, Pluvio, [4]Temp	0.86	0.05	[1]pH, EC, NO_3^-, DO, Disch, [6]Month	0.95	0.07	[1]PO_4^{3-}, EC, Pluvio, Chl-*a*, [5]Month	0.73	0.07

Sal salinity, *Disch* river discharge, *Pluvio* pluviometry, *Temp* water temperature

Table 5 Sorted rotated factor loadings (Varimax normalized) of data in the three principal factors derived from the principal component analysis (PCA) for the Comoé, Bandama and Bia Rivers

	Dry season			Rainy season			Flood season		
	Fact. 1	Fact. 2	Fact. 3	Fact. 1	Fact. 2	Fact. 3	Fact. 1	Fact. 2	Fact. 3
Pluviometry	−0.90	0.37	−0.08	−0.76	0.41	0.25	−0.83	0.40	−0.32
Temperature	0.78	−0.34	−0.22	−0.43	0.38	0.60	0.49	−0.69	−0.13
pH	−0.30	−0.90	0.10	−0.24	0.28	−0.22	−0.59	0.17	0.25
EC	0.79	0.37	0.11	−0.87	−0.42	0.14	0.65	0.61	0.33
DO	−0.08	−0.80	0.51	0.64	0.15	0.50	0.21	0.06	−0.72
Salinity	0.77	0.32	0.31	−0.83	−0.49	0.16	0.65	0.61	0.32
Chl-*a*	0.30	0.51	0.11	−0.38	−0.19	−0.54	0.52	0.08	−0.49
NH_4^+	−0.06	−0.41	−0.39	−0.33	0.56	−0.68	−0.51	−0.26	0.36
PO_4^{3-}	−0.58	0.08	0.49	−0.26	−0.84	−0.26	−0.41	−0.52	0.29
NO_3^-	−0.02	0.15	0.71	−0.36	0.75	−0.38	−0.11	0.94	0.02
River discharge	0.84	−0.47	0.10	−0.61	0.26	0.50	0.85	−0.37	0.28
Eigen value	3.87	2.62	1.35	3.48	2.53	1.99	3.60	2.78	1.44
Cumulative %	35.2	59.0	71.3	31.7	54.6	72.7	32.8	58.1	71.2

Table 6 Characteristics of the models obtained for each river

River	Static					Dynamic (t)					Dynamic (t + 1)				
	Network model	R_{app}	R_{val}	MSE_{val}	BIC	Network model	R_{app}	R_{val}	MSE_{val}	BIC	Network model	R_{app}	R_{val}	MSE_{val}	BIC
Comoé	5–5 - 1*	0.96	0.75	0.09	−1.01	4–6 - 1	0.90	0.82	0.11	−0.90	5–3 - 1	0.88	0.63	0.13	−0.85
Bandama	6–5 - 1	0.91	0.67	0.15	−0.78	5–3 - 1	0.85	0.66	0.22	−0.63	6–6 - 1	0.93	0.67	0.21	−0.64
Bia	4–4 - 1	0.87	0.86	0.05	−1.24	6–5 - 1	0.98	0.95	0.07	−1.15	5–4 - 1	0.90	0.73	0.07	−1.11

*The 5–5 - 1 architecture translates 5 neurons in input layer (X_i), 5 nodes in hidden layer and 1 neuron for output (Chl-*a*)

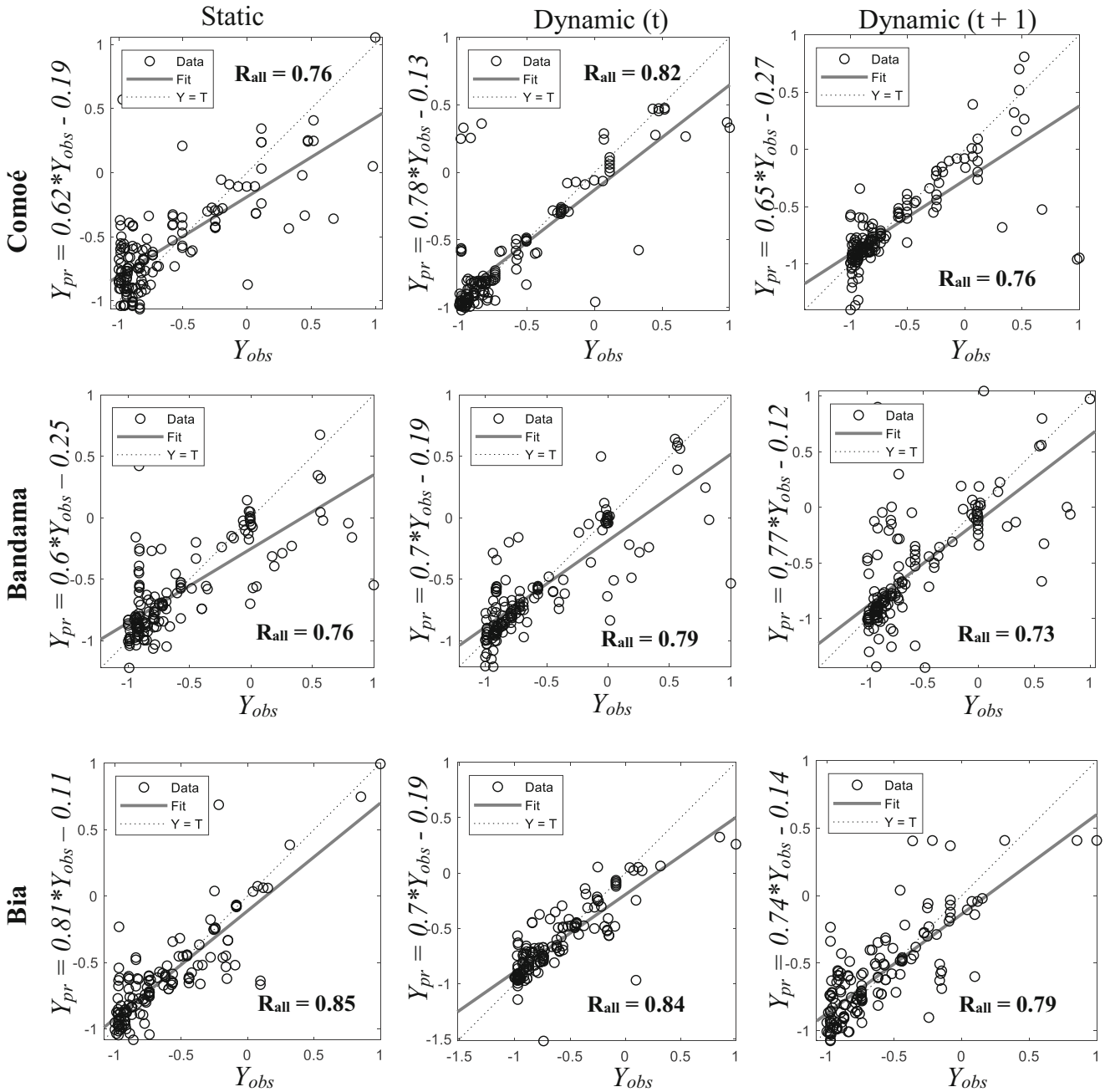

Fig. 6 Comparison of experimental and predicted data obtained from ANN

phosphorus in the Bandama and Bia Rivers, respectively, during the rainy season. Overall, the map distributions and the presence of associations between the chlorophyll-*a* abundance with the environmental parameters measured, show that chlorophyll-*a* dynamics in the rivers could be dictated by nitrates and phosphates availability, point sources and diffuse sources as well as the river flow.

Eutrophication State

The trophic status of the rivers was assessed using the classification scheme for Chl-*a* biomass (EEA 2001). The water quality of the Comoé, Bandama and Bia Rivers was most often under the mesotrophic state during the three sampling seasons (Table 3). This finding confirms our rationale that high nutrient concentrations result in sometimes a hypereutrophic state of the rivers, especially during the flood season as revealed by the significant correlations obtained between nutrients and algae (Chl-*a*). In addition, during the dry and rainy seasons, abundant sunlight, water temperature and aquatic chemistry create an ideal environment for algae growth. Algae blooms in rivers in summers were related to nutrient enrichment, especially in nitrogen and phosphorus from primarily agriculture non-point pollution (Wang et al. 2004; Zhang et al. 2011).

Predictive Power

The relative importance of the predictor values in the best performing ANNs was estimated using the Olden method (Olden et al. 2004) (Fig.5). The further away from zero, the more important the predictor was, regardless of sign. Given the performance of static modeling of Chl-*a* in the three rivers, the high scores R_{val} (range: 0.67 to 0.86) and the low MSE_{val} (range: 0.05 to 0.15) testified to the accuracy of ANN networks obtained with at most six predictors such as water salinity, EC, temperature, PO_4^{3-}, pluviometry, NO_3^- (Table 4). Although the predictor importance varied among these

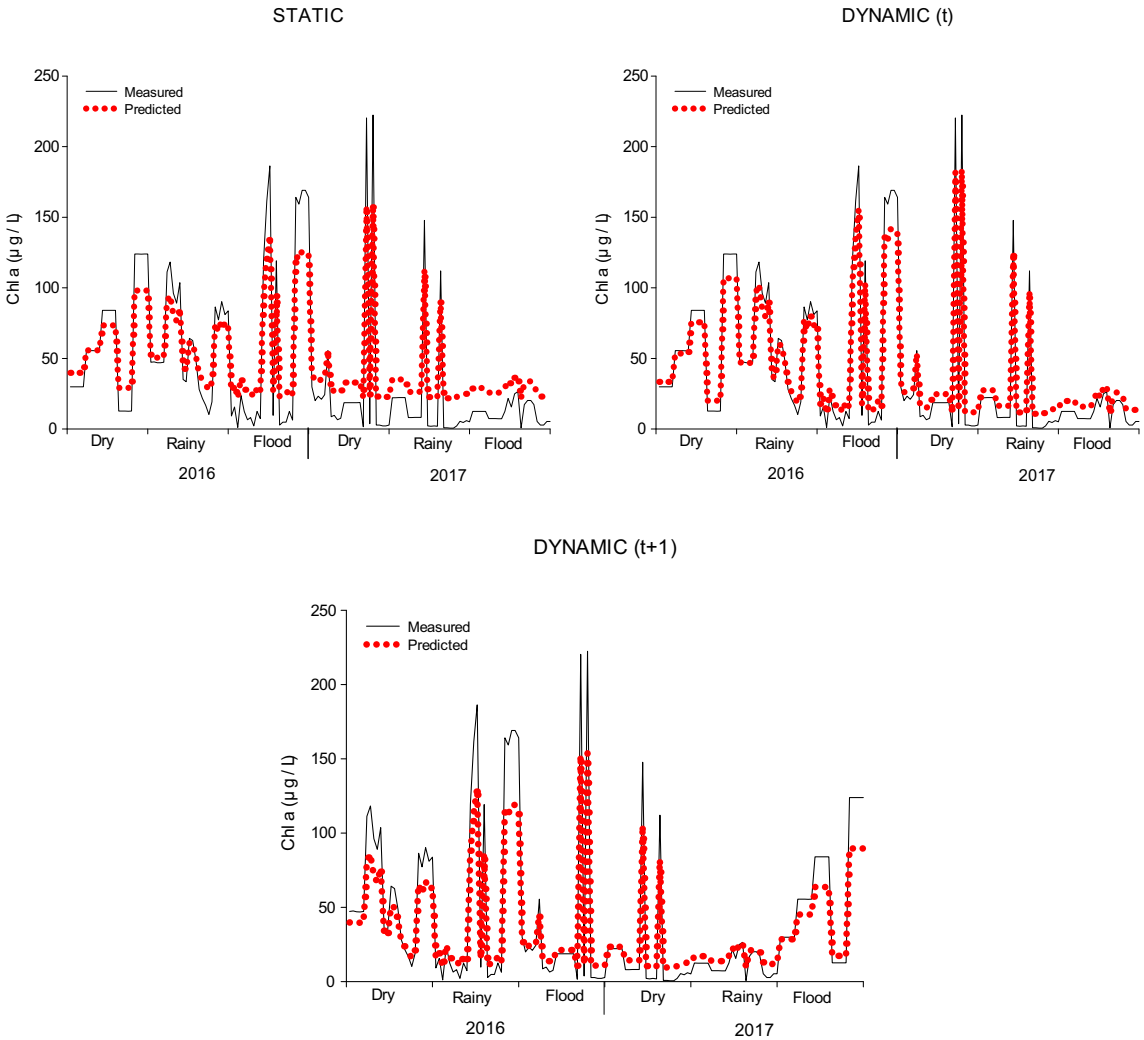

Fig. 7 Measured and predicted values of Chlorophyll-*a* from static and dynamic approaches in the Comoé River

networks, the overall ranking of the predictors was conserved. Four to six predictors forecasted the measured Chl-*a* values using the dynamic approaches. The high scores R_{val} (range: 0.63 to 0.95) and the low MSE_{val} (range: 0.07 to 0.22) supported the accuracy of the obtained ANN networks.

A PCA analysis was performed on the samples collected from all rivers and seasons (the dry, rainy and flood seasons) to examine factors driving the distribution of the studied parameters in the rivers (Table 5). The results showed three significant components for each season, accounting for 71.3, 72.7 and 71.2%, respectively, of the total variances of information contained in the original dataset. Water EC, salinity, pluviometry and river discharge showed high loadings (absolute weight > 0.6) on factor 1 during the three seasons. Moreover, the Pearson correlations showed linear associations between river discharge with pluviometry, EC and water salinity, but there was no linear association of these parameters with Chl-*a*. The factor 1 shows that pluviometry (rainfall) may drive the distribution of water EC, salinity, and river discharge in the rivers.

Factor 2 showed high loadings (absolute weight > 0.6) with pH and DO during the dry season, with PO_4^{3-} and NO_3^- during the rainy season, and with NO_3^- and temperature during the flood season. Moreover, the Pearson correlations showed linear associations between PO_4^{3-} and Chl-*a* in the Bandama (r = 0.29) and Bia (r = 0.43) Rivers, while NO_3^- and Chl-*a* had linear association in the Comoé River (r = 0.37). The rainy and flood seasons caused excess phosphorus and nitrate inputs probably through soil erosion; this may lead to hyperfertilization of the environment and an increase in primary production (Gladyshev and Gubelitc 2019). So, factor 2 shows that PO_4^{3-} and NO_3^- impact chlorophyll-*a* abundance.

Factor 3 showed high loadings (absolute weight > 0.6) with NO_3^- during the dry season; with NH_4^+ during the rainy season, and with DO during the flood season. This factor shows that DO and NO_3^- and NH_4^+ ions may impact chlorophyll-*a* abundance. Algal growth in the aquatic system was also accompanied by a drop in oxygen demand, as example in the Bia River where a negative linear correlation between Chl-*a*

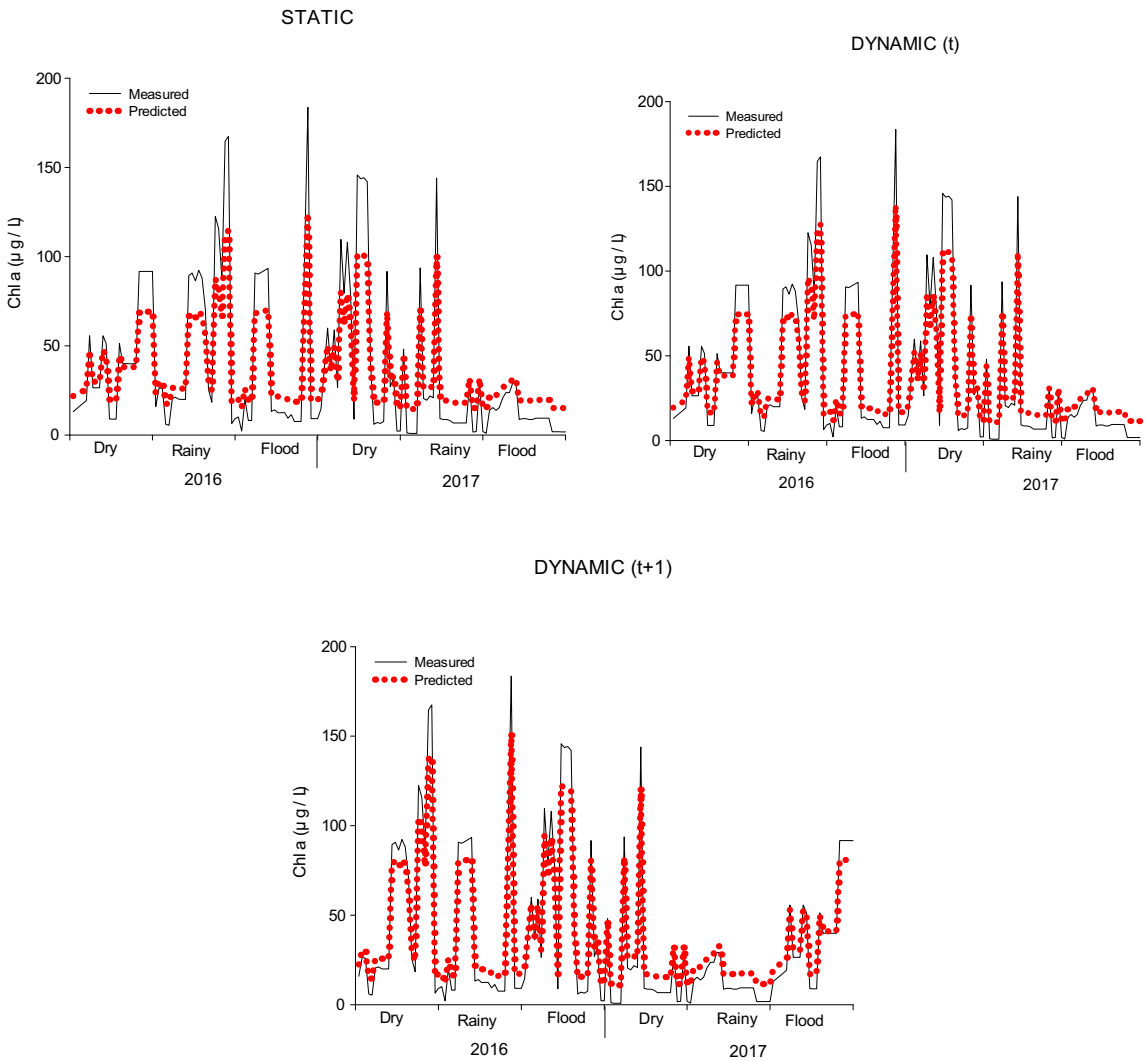

Fig. 8 Measured and predicted values of Chlorophyll-*a* from static and dynamic approaches in the Bandama River

and DO was obtained (r = − 0.18). Overall, the PCA results show that rainfall and the seasons play a key role on the distribution of the physical and chemical parameters in the rivers.

Chlorophyll-*a* Prediction

The highest R_{app} and R_{val} values corresponding to the lowest MSE_{val} and BICs of each river are recorded in Table 6. The correlation coefficient R_{app} varied from 0.85 to 0.98 for the training subset, while the correlation coefficient R_{val} varied from 0.63 to 0.95 for the validation subset. Further, the choice of potentially generalizable ANN models was made taking into account the lower values of MSE_{val} (0.05 to 0.22) and the BIC (< − 0.5). These results allowed to identify the models of the network architecture (Ngoran et al. 2009; Yao et al. 2017) that can simulate the dynamics of chlorophyll-*a* in the Comoé, Bandama and Bia Rivers, according to both approaches (i.e., static and dynamic). Yet, since the best network model is a compromise between the results obtained during the computing process (training and validation) and the adequacy of the simulated and observed values, regression plots were constructed to compare experimental and predicted data of chlorophyll-*a* in the three rivers (Fig. 6). Y_{obs} is the target variable (i.e., measured chlorophyll-*a*) and Y_{pr} is the simulated variable (i.e., predicted chlorophyll-*a*). Each graph consists of one dashed line called a best-fit line (y = T, i.e., predicted = experimental data) with a correlation value (R_{all}) on the plot. The best generalizable models are the ones that predict more than 50% ($R_{all} > 0.5$) of the chlorophyll-*a* value (Mandal et al. 2015).

As shown in Figs. 6 and 7, the 5–5 - 1 model predicted 76% of the static evolution of chlorophyll-*a*, while the 4–6 - 1 and 5–3 - 1 models predicted 82% and 76%, respectively, of the dynamic evolution of chlorophyll-*a* at season (t) and the next season (t + 1), in the Comoé River. Overall, the high R_{app} (> 0.85) and R_{val} (> 0.60) scores presented in Table 6 and the low discrepancies between expected and observed values displayed in Fig. 7 are indicative of a good prediction of the chlorophyll-*a* in this river by ANNs models.

With regard to the Bandama River, the 6–5 - 1 model predicted 76% of the static evolution of chlorophyll-*a*, while the 5–3 - 1 and 6–6 - 1 models predicted 79% and 73%, respectively, of the

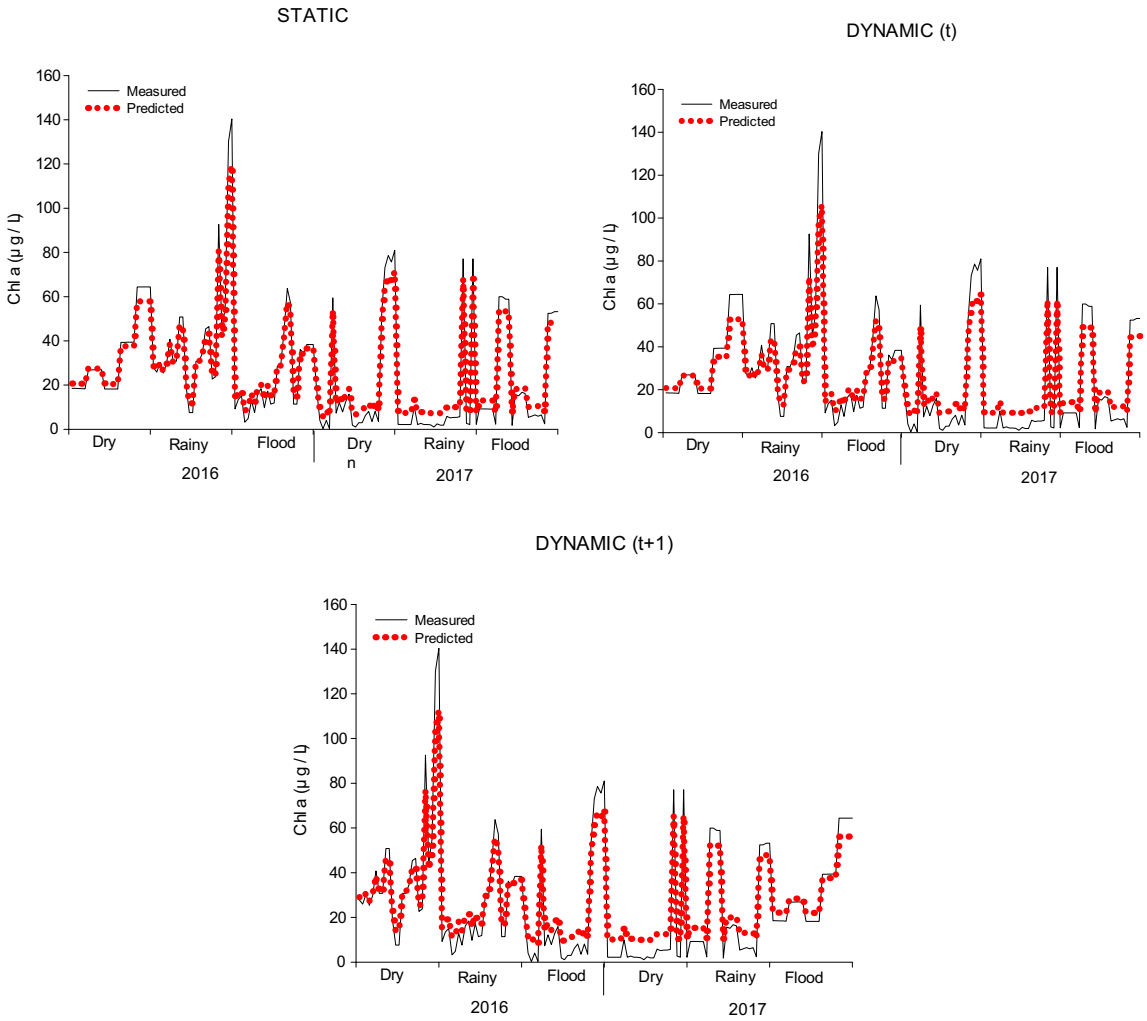

Fig. 9 Measured and predicted values of Chlorophyll-*a* from static and dynamic approaches in the Bia River

dynamic evolution of chlorophyll-*a* at season (t) and the next season (t + 1). This is supported by Fig. 8 on which the static and dynamics (t and t + 1) approach curves showed very similar values between predicted and field measurements. Moreover the high R_{app} (> 0.85) and R_{val} (> 0.65) scores presented in Table 6 and the low discrepancies between expected and observed values displayed in Fig. 6 are indicative of the good prediction of the Chlorophyll-*a* in this river by ANNs models.

As for the Bia River, the 4–4 - 1 model predicted 85% of the static evolution of chlorophyll-*a*, while the 6–5 - 1 and 5–4 - 1 models predicted 84% and 79% of the dynamics of chlorophyll-*a* at season (t) and the next season (t + 1), respectively. As seen on Fig. 9, the static and dynamic approach curves predicted chlorophyll-*a* values very close to the field data. Moreover the high R_{app} (> 0.85) and R_{val} (> 0.70) scores presented in Table 6 and the low discrepancies between expected and observed values displayed in Fig. 6 are indicative of the good prediction of the Chlorophyll-*a* in this river by ANNs models.

In general, the ANN models showed a high degree of consistency between the field and prediction data.

The Bia River MREs were 3.90, 3.66, and 5.27%, respectively, for the static and dynamic approaches (t and t + 1), indicating low difference between the outputs of the ANN models and field data. Therefore, the 4–4 - 1, 6–5 - 1 and 5–4 - 1 models are generalizable for the Bia River (Table 7). The same was true for the 6–5 - 1, 5–3 - 1 and 6–6 - 1 models in the Bandama River with MRE values of 4.58, 3.95 and 3.70%, respectively, and for the 5–5 - 1, 4–6 - 1 and 5–3 - 1 models in the Comoé River with MRE values of 7.71, 5.51 and 3.22%, respectively.

This study revealed nine best neural networks for forecasting Chl-*a* concentrations in the Comoé, Bandama and Bia Rivers. The neural networks were successful in modeling between 73 and 85% of the response (chlorophyll-*a* concentration) with at most six predictor variables. The network performance was relatively comparable to that of ANNs built by Coutinho et al. (2019) (82%) to model Chl-*a* abundance in Guanabara Bay, Rio de Janeiro using water temperature, transparency, total nitrogen, total phosphorus, and salinity as relevant predictors and by Flombaum et al. (2013) (68%) to model microbial abundance in the Global Ocean. Therefore, the neural network approach is a successful method of modeling such complex and non-linear phenomena as algal blooms in freshwater systems with different environmental conditions. Thus, the hypothesis that ecosystem processes are best modeled when non-linearity of relationships is assumed is retained (Recknagel et al. 1997; Wilson and Recknagel 2001). Yet, Recknagel et al. (2002) and Park et al. (2015) showed that artificial neural network models can be powerful short-term predictors of the timing of algal bloom events but are difficult to generalize and do not provide explicit explanation of underlying processes. The differences in the precision observed for the nine final networks in the present study could have been due to the need to include biotic predictors in modeling the response (Tromas et al. 2017).

Table 7 Performance of the ANN models obtained

Model validation parameter	Comoé			Bandama			Bia		
	Static 5–5 - 1	Dynamic (t) 4–6 - 1	Dynamic (t + 1) 5–3 - 1	Static 6–5 - 1	Dynamic (t) 5–3 - 1	Dynamic (t + 1) 6–6 - 1	Static 4–4 - 1	Dynamic (t) 6–5 - 1	Dynamic (t + 1) 5–4 - 1
Correlation value (R_{all})	> 0.5	> 0.5	> 0.5	> 0.5	> 0.5	> 0.5	> 0.5	> 0.5	> 0.5
MRE (%)	7.71	5.51	3.22	4.58	3.95	3.70	3.90	3.66	5.27
MRE state	Low	Low	Low	Low	Low	Low	Low	Low	Low
Model performance	Generalizable	Generalizable	Generalizable	Generalizable	Generalizable	Generalizable	Generalizable	Generalizable	Generalizable

Environmental Significance

Results from this study demonstrate that the Comoé, Bandama and Bia Rivers are in an advanced eutrophication state, based on Chl-*a* observations over 2 years. A number of environmental parameters such as water temperature, pH, EC, salinity, PO_4^{3-}, and river discharge were found as significant drivers of chlorophyll-*a* concentration depending on the river.

Overall, the ANN model simulations data fitted accurately the field measurements; therefore, they can be useful as alert tool for decision-makers in the monitoring of chlorophyll-*a* (thus, the eutrophication phenomenon) evolution in the Comoé, Bia and Bandama Rivers.

Conclusion

The monitoring of riverine water eutrophication state in West Africa represents a major challenge for the leaders as these waters are vital for the subsistence of populations. This study revealed that chlorophyll-*a* dynamic in the Comoé, Bandama and Bia Rivers was characterized by higher levels upstream during the rainy season as well as very high values downstream in the estuarine parts during the dry, rainy and flood seasons. Chlorophyll-*a* concentrations in the rivers resulted mainly from anthropogenic inputs such as agricultural and urban runoffs, leading to a progressive deterioration of the waters. Artificial neural network (ANN) models predicted up to 85% of the chlorophyll-*a* concentrations in the rivers with satisfactory accuracy. Therefore, the result of this study demonstrates that the degree of eutrophication in tropical rivers can be predicted successfully using ANN models with few data in the field, which could benefit river management with less cost for water quality monitoring. It should be appropriate to raise awareness of the populations on the moderate use of agricultural inputs in order to reduce water eutrophication.

Acknowledgments The authors are thankful to the Director of Centre de Recherches Océanologiques (CRO) for his encouragement and support. Special thanks are expressed to the reviewers for their critical contribution.

Data Availability Raw data have been deposited supplementary files.

Compliance with Ethical Standards

Conflict to Interest The authors declare that they have no conflict to interest.

References

Aguiar VMC, Neto JAB, Rangel CM (2011) Eutrophication and hypoxia in four streams discharging in Guanabara Bay, RJ, Brazil, a case study. Marine Pollution Bulletin 62:1915–1919

Assidjo E, Yao B, Kisselmina K, Amané D (2008) Modeling of an industrial drying process by artificial neural networks. Brazilian Journal of Chemical Engineering 25(03):515–522

Awad M (2014) Sea water chlorophyll-a estimation using hyperspectral images and supervised artificial neural network. Ecological Informatics 24:60–68

Chang NB, Mohiuddin G, Crawford AJ, Bai K, Jin KR (2015) Diagnosis of the artificial intelligence-based predictions of flow regime in a constructed wetland for storm water pollution control. Ecological Informatics 28:42–60

Chen X, Jiang H, Sun X, Zhu Y, Yang L (2016) Nitrification and denitrification by algae-attached and free living microorganisms during a cyanobacterial bloom in Lake Taihu, a shallow eutrophic Lake in China. Biogeochemical 131:135–146

Chen Y, Yu H, Cheng Y, Cheng Q, Li D (2018) A hybrid intelligent method for three-dimensional short-term prediction of dissolved oxygen content in aquaculture. PLoS One 13(2):e0192456

Coutinho FH, Thompson CC, Cabral AS, Paranhos R, Dutilh BE, Thompson FL (2019) Modelling the influence of environmental parameters over marine planktonic microbial communities using artificial neural networks. Science of the Total Environment 677: 205–214

Cunha DGF, Calijuri MC, Lamparelli MC (2013) A trophic state index for tropical/subtropical reservoirs (TSItsr). Ecological Engineering 60:126–134

de Sousa Barroso H, Becker H, VMM M (2016) Influence of river discharge on phytoplankton structure and nutrient concentrations in four tropical semiarid estuaries. Brazilian Journal of Oceanography 64(1):37–48

Durand JR, Dufour P, Guiral D, Zabi SGF (1994) Environment and aquatic resources of Ivory Coast: the lagoon environments (in French). ORSTOM (ed, vol 2), Ivory Coast

EEA, European Environment Agency (2001) Eutrophication in Europe's coastal waters Topic report No. 7, Copenhagen, p. 86

Flombaum P, Gallegos JL, Gordillo R, Rincón J, Zabala LL, Jiao N (2013) Present and future global distributions of the marine cyanobacteria Prochlrococcus and Synechococcus. PNAS 110: 9824–9829

Gibson G, Carlson R, Simpson J, Smeltzer E (2000) Nutrient criteria technical guidance manual: lakes and reservoirs (EPA-822-B00–001). United States Environment Protection Agency, Washington DC, 232 p

Girard G, Sircoulon J, Touchebeuf P (1970) Overview of the hydrological regimes of Ivory Coast (in French). ORSTOM (ed), Ivory Coast

Gladyshev MI, Gubelitc YI (2019) Green tides: new consequences of the eutrophication of natural waters (invited review). Contemporary Problems of Ecology 12:2109–2125

Grasshoff K, Ehrhardt M, Kremling K (1999) Methods of seawater analysis. Third (ed), Weinhein

Hao Q, Chai F, Xiu P, Bai Y, Chen J, Liu C, Le F, Zhou F (2019) Spatial and temporal variation in chlorophyll *a* concentration in the eastern China seas based on a locally modified satellite dataset. Estuarine, Coastal and Shelf Science 220:220–231

Huang J, Gao J (2017) An ensemble simulation approach for artificial neural network: an example from chlorophyll *a* simulation in Lake Poyang, China. Ecological Informatics 37:52–58

Huo S, He Z, Su J, Xi B, Zhu C (2013) Using artificial neural network models for eutrophication prediction. Procedia Environmental Sciences 18:310–316

Jin XC, Tu QY (1990) Investigate specification of Lake eutrophication. China Environmental Science Press, Beijing

Koroleff F (1970) Revised version of direct determination of ammonia in natural waters as indophenol blue. Int con Explor Sea C. M. 1969/C in: 9 ICES information on techniques and methods for sea water analysis. Interlab Rep 3, pp 19–22

Le Moal M, Gascuel-Odoux C, Ménesguen A, Souchond Y, Étrillard C, Levain A, Moatar F, Pannard A, Souchu P, Lefebvre A, Pinay G (2019) Eutrophication: a new wine in an old bottle? Science of the Total Environment 651:1–11

Lee KY, Chung N, Hwang S (2016) Application of an artificial neural network (ANN) model for predicting mosquito abundances in urban areas. Ecological Informatics 36:172–180

Levenberg K (1944) A method for the solution of certain problems in least squares. Quarterly of Applied Mathematics 2:164–168

Li W, Cui L, Zhang Y, Zhang M, Zhao X, Wang Y (2013) Statistical modeling of phosphorus removal in horizontal subsurface constructed wetland. Wetlands 34:427–437

Li X, Sha J, Wang Z-L (2017) Chlorophyll-a prediction of lakes with different water quality patterns in China based on hybrid neural networks. Water 9:524

Lohani AK, Goel NK, Bhatia KKS (2011) Comparative study of neural network, fuzzy logic and linear transfer function techniques in daily rainfall-runoff modelling under different input domains. Hydrological Processes 25(2):175–193

Lorenzen CJ (1967) Determination of chlorophyll and pheo-pigments: spectrophotometric equations. Tuna Ocean research program 14-17-0007-458:343–346

Mandal S, Mahapatra SS, Patel RK (2015) Enhanced removal of Cr (VI) by cerium oxide polyaniline composite: optimization and modeling approach using response surface methodology and artificial neural networks. Journal of Environmental Chemical Engineering 3(2): 870–885

Marquardt D (1963) An algorithm for least-squares estimation of nonlinear parameters. Journal of the Society for Industrial and Applied Mathematics 11:431–441

Moscuzza C, Volpedo AV, Ojeda C, Cirelli AF (2007) Water quality index as a tool for river assessment in agricultural areas in the Pampean plains of Argentina. Journal of Environmental Engineering 1:18–25

Muller AC, Muller DL (2015) Forecasting future estuarine hypoxia using a wavelet based neural network model. Ocean Modelling 96(2): 314–323

Murphy J, Riley JP (1962) A modified solution method for determination of phosphate in natural waters. Analytica Chimica Acta 27:31–36

N'Goran KM, Yao KM, Kouassi NLB, Trokourey A (2019) Phosphorus and nitrogen speciation in waters and sediments highly contaminated by an illicit urban landfill: the Akouedo landfill, Côte d'Ivoire. Regional Studies in Marine Science 31:100805

Ngoran EBZ, Assidjo NE, Kouamé P, Dembele I, Yao B (2009) Modelling of osmotic dehydration of mango (MangiferaIndica) by recurrent artificial neural network and experimental design. Research Journal of Agriculture and Biological Sciences 5(5):754–761

Olden JD, Joy MK, Death RG (2004) An accurate comparison of methods for quantifying variable importance in artificial neural networks using simulated data. Ecological Modelling 178:389–397

Ota M, Takenaka M, Sato Y, Smith RL Jr, Inomata H (2015) Effects of light intensity and temperature on photoautotrophic growth of a green microalga, *Chlorococcumlittorale*. Biotechnology Reports 7: 24–29

Park Y, Cho KH, Park J, Cha SM, Kim JH (2015) Development of early-warning protocol for predicting chlorophyll-a concentration using machine learning models in freshwater and estuarine reservoirs, Korea. Science of the Total Environment 502:31–41

Pesce SF, Wunderlin DA (2000) Use of water quality indices to verify the impact of Córdoba City (Argentina) on Suquía River. Water Research 34(11):2915–2926

Pettine M, Casentini B, Fazi S, Giovanardi F, Pagnotta R (2007) A revisitation of TRIX for trophic status assessment in the light of the European water framework directive: application to Italian coastal waters. Marine Pollution Bulletin 54:1413–1426

Primpas I, Karydis M (2010) Scaling the trophic index (TRIX) in oligotrophic marine environments. Environmental Monitoring and Assessment 178:257–269

Recknagel F, French M, Harkonen P, Yabunaka KI (1997) Artificial neural network approach for modelling and prediction of algal blooms. Ecological Modelling 96:11–28

Recknagel F, Bobbin J, Whigham P, Wilson H (2002) Comparative application of artificial neural networks and genetic algorithms for multivariate time-series modelling of algal blooms in freshwater lakes. Journal of Hydroinformatics 4:125–133

Rodier J, Legube B, Merlet N *et coll.* (2009) Water analysis (in French). 9th edition, DUNOD, Paris

Schwarz G (1978) The annals of statistics. In: Estimating the dimension of a model, pp 461-464 (vol 6, 2)

Singh SP, Singh P (2015) Effect of temperature and light on the growth of algae species: a review. Renewable and Sustainable Energy Reviews 50:431–444

Sudheer KP, Jain A (2004) Explaining the internal behavior of artificial neural network river flow models. Hydrological Processes 18(4): 833–844

Sudheer KP, Gosain AK, Ramasastri KS (2002) A data-driven algorithm for constructing artificial neural network rainfall-runoff models. Hydrological Processes 16(6):1325–1330

Svirčev Z, Krstič S, Miladinov-mikov M, Baltič V, Vidovič M (2009) Freshwater Cyanobacterial blooms and primary liver Cancer epidemiological studies in Serbia. Journal of Environmental Science and Health Part C: Environmental Arcinogenesis and Ecotoxicology Reviews 27(1):36–55

Tian W, Liao Z, Zhang J (2017) An optimization of artificial neural network model for predicting chlorophyll dynamics. Ecological Modelling 364:42–52

Tromas N, Fortin N, Bedrani L, Terrat Y, Cardoso P, Bird D (2017) Characterising and predicting cyanobacterial blooms in an 8-year amplicon sequencing time course. The ISME Journal 11:1746–1763

Wang XJ, Zhang W, Huang YN, Li S (2004) Modeling and simulation of point-non-point source effluent trading in Taihu Lake area: perspective of non-point sources control in China. Journal of Science of the Total Environment 325:39–50

Wang H, Yan X, Chen H, Chen C, Guo M (2015) Chlorophyll-a predicting model based on dynamic neural network. Applied Artificial Intelligence 29(10):962–978

Wilson H, Recknagel F (2001) Towards a generic artificial neural network model for dynamic predictions of algal abundance in freshwater lakes. Ecological Modelling 146:69–84

Wu N, Huang J, Schmalz B, Fohrer N (2013) Modeling daily chlorophyll a dynamics in a German lowland river using artificial neural networks and multiple linear regression approaches. Limnology 15(1): 47–56

Wu Z, He H, Cai Y, Zhang L, Chen Y (2014) Spatial distribution of chlorophyll a and its relationship with the environment during summer in Lake Poyang: a Yangtze-connected lake. Hydrobiologia 732(1):61–70

Wu Z, Wang X, Chen Y, Cai Y, Deng J (2018) Assessing river water quality using water quality index in Lake Taihu Basin, China. Science of the Total Environment 612:914–922

Xu Y, Ma C, Liu Q, Xi B, Qian G, Zhang D, Huo S (2015) Method to predict key factors affecting lake eutrophication - a new approach based on support vector regression model. International Biodeterioration and Biodegradation 102:308–315

Yao MK, Akmel D, Akpetou K, Trokourey A, Yao K, Assidjo N (2017) Modeling the spatio-temporal evolution of mineral phosphorus in a tropical hypereutrophic lagoon bay: the

Tiagba lagoon bay (Ivory Coast) (in French). Journal of Water Science 30(3):247–258

Yasin JA, Kroeze C, Mayorga E (2010) Nutrients export by rivers to the coastal waters of Africa: past and future trends. Global Biogeochemical Cycles 24:GB0A07

Zhang J, Ni W, Luo Y, Stevenson RJ, Qi J (2011) Response of freshwater algae to water quality in Qinshan Lake within Taihu watershed, China. Physics and Chemistry of the Earth 36:360–365